

# **Sensitivity of Middle Atmospheric Temperature and Circulation in the UIUC Mesosphere-Stratosphere-Troposphere GCM to the Treatment of Subgrid-Scale Gravity-Wave Breaking**

*Fanglin Yang, Michael E. Schlesinger, Natasha Andronova, Vladimir A. Zubov,  
Eugene V. Rozanov, Lin B. Callis*

To be submitted to Journal of Geophysical Research

## **ABSTRACT**

The sensitivity of the middle atmospheric temperature and circulation to the treatment of mean-flow forcing due to breaking gravity waves was investigated using the University of Illinois at Urbana-Champaign 40-layer Mesosphere-Stratosphere-Troposphere General Circulation Model (MST-GCM). Three GCM experiments were performed. The gravity-wave forcing was represented first by Rayleigh friction, and then by the *Alexander and Dunkerton* (AD) parameterization with weak and strong breaking effects of gravity waves. In all experiments, the *Palmer et al.* parameterization was included to treat the breaking of topographic gravity waves in the troposphere and lower stratosphere. Overall, the experiment with the strong breaking effect simulates best the middle atmospheric temperature and circulation. With Rayleigh friction and the weak breaking effect, a large warm bias of up to 60°C was found in the summer upper mesosphere and lower thermosphere. This warm bias was linked to the inability of the GCM to simulate the reversal of the zonal winds from easterly to westerly crossing the mesopause in the summer hemisphere. With the strong breaking effect, the GCM was able to simulate this reversal, and essentially eliminated the warm bias. This improvement was the result of a much stronger meridional transport circulation that possesses a strong vertical ascending branch in the summer upper mesosphere, and hence large adiabatic cooling. Budget analysis indicates that in the middle atmosphere the forces that act to maintain a steady zonal-mean zonal wind are primarily those associated with the meridional transport circulation and breaking gravity waves. Contributions from the interaction of the model-resolved eddies with the mean flow are small. To obtain a transport circulation in the mesosphere of the UIUC MST-GCM that is strong enough to produce the observed cold summer mesopause, gravity-wave forcing larger than 100 m/s/day in magnitude is required near the summer mesopause. In the tropics, only with the AD parameterization can the model produce realistic semiannual oscillations.

**Sensitivity of Middle Atmospheric Temperature and Circulation in  
the UIUC Mesosphere-Stratosphere-Troposphere GCM to the  
Treatment of Subgrid-Scale Gravity-Wave Breaking**

Fanglin Yang<sup>1</sup>, Michael E. Schlesinger<sup>2</sup>, Natasha Andronova<sup>2</sup>, Vladimir A. Zubov<sup>3</sup>,  
Eugene V. Rozanov<sup>4</sup>, Lin B. Callis<sup>5</sup>

1. Goddard Earth Sciences and Technology Center, University of Maryland Baltimore County, Baltimore, MD 21250
2. Climate Research Group, Department of Atmospheric Sciences, University of Illinois at Urbana-Champaign, 105 S. Gregory Street, Urbana, Illinois 61801, USA
3. A. I. Voeikov Main Geophysical Observatory, 7 Karbyshev Street, St. Petersburg, 194021, Russia
4. PMOD/WRC and IAC ETHZ, Dorfstrasse 33, Davos Dorf, CH-7260, Switzerland
5. Consultant, 613 West Riverview Dr., Suffolk, VA 23434, USA

## ABSTRACT

The sensitivity of the middle atmospheric temperature and circulation to the treatment of mean-flow forcing due to breaking gravity waves was investigated using the University of Illinois at Urbana-Champaign 40-layer Mesosphere-Stratosphere-Troposphere General Circulation Model (MST-GCM). Three GCM experiments were performed. The gravity-wave forcing was represented first by Rayleigh friction, and then by the *Alexander and Dunkerton* (AD) parameterization with weak and strong breaking effects of gravity waves. In all experiments, the *Palmer et al.* parameterization was included to treat the breaking of topographic gravity waves in the troposphere and lower stratosphere. Overall, the experiment with the strong breaking effect simulates best the middle atmospheric temperature and circulation. With Rayleigh friction and the weak breaking effect, a large warm bias of up to 60°C was found in the summer upper mesosphere and lower thermosphere. This warm bias was linked to the inability of the GCM to simulate the reversal of the zonal winds from easterly to westerly crossing the mesopause in the summer hemisphere. With the strong breaking effect, the GCM was able to simulate this reversal, and essentially eliminated the warm bias. This improvement was the result of a much stronger meridional transport circulation that possesses a strong vertical ascending branch in the summer upper mesosphere, and hence large adiabatic cooling. Budget analysis indicates that in the middle atmosphere the forces that act to maintain a steady zonal-mean zonal wind are primarily those associated with the meridional transport circulation and breaking gravity waves. Contributions from the interaction of the model-resolved eddies with the mean flow are small. To obtain a transport circulation in the mesosphere of the UIUC MST-GCM that is strong enough to produce the observed cold summer mesopause, gravity-wave forcing larger than 100 m/s/day in magnitude is required near the summer mesopause. In the

tropics, only with the AD parameterization can the model produce realistic semiannual oscillations.

## 1. Introduction

It has long been recognized that atmospheric gravity waves have strong effects on atmospheric temperature and circulation. They transport energy and momentum, produce turbulence and mixing, and modify the mean circulation and thermal structure of the atmosphere (for a review see *Fritts and Alexander* [2003] and references therein). In the past two decades a number of schemes [e.g., *Palmer et al.* 1986; *McFarlane*, 1987; *Fritts and Lu*, 1993; *Lott and Miller*, 1997] have emerged that parameterize the drag effect of topographic (stationary) gravity waves on the mean flow in atmospheric general circulation models (GCM). Almost all current atmospheric GCMs have adopted some scheme to treat topographic gravity-wave forcing in the troposphere and lower stratosphere, and for some cases through the entire atmosphere. GCMs including these schemes are able to simulate much better the troposphere jets, sea-level pressure and surface winds in the northern middle to high latitudes [*Hamilton*, 1997]. However, the progress in developing parameterization schemes for either stationary or non-stationary gravity waves suitable for use in the middle atmosphere has been relatively slow due to limitations in both theoretical understanding and field observations. Accordingly, Rayleigh friction was chosen by many GCM modelers to treat crudely the forcing effects of breaking gravity waves in the middle atmosphere [e.g., *Boville*, 1995; *Beagley et al.*, 1996; *Manzini and Bengtsson*, 1996; *Langematz and Pawson*, 1997; *Swinbank et al.*, 1998]. In recent years however, considerable advances have been made in the observation, theoretical understanding and modeling of middle atmospheric gravity waves [*Fritts and Alexander*, 2003]. The advances have led to a number of parameterizations that are applicable for GCMs to describe the forcing by gravity-wave breaking on the large-scale circulation in the middle atmosphere [e.g., *Medvedev and Klaasen*, 1995;

*Hines*, 1997a,b; *Alexander and Dunkerton*, 1999; *Warner and McIntyre*, 2001]. Many of these schemes are now in different stages of testing and implementation by GCM groups.

At the University of Illinois at Urbana-Champaign (UIUC) a 40-layer mesosphere-stratosphere-troposphere general circulation model (MST-GCM) was developed based on the UIUC 24-layer stratosphere-troposphere (ST) GCM [*Yang et al.*, 2000]. This 40-layer GCM extends up to the lower thermosphere with its top at 0.00084 hPa (about 98 km). One application of the GCM is to study the impact of solar variability on atmospheric chemical composition and climate. Special attention has been paid to the simulation of upper atmospheric temperature and circulation because they influence atmospheric chemical reactions and the transport of atmospheric constituents. To parameterize the forcing of breaking gravity waves on the mean flow in the middle atmosphere, the scheme of Rayleigh friction, which was introduced by *Holton and Wehrbein* [1980] and used in the UIUC 24-layer GCM, was first expanded and tested. Unsatisfied with the outcome, we have adopted the more physically based yet relatively simple parameterization developed by *Alexander and Dunkerton* [1999] (hereinafter referred to as AD). Here we document two experiments using the AD parameterization, along with the case of Rayleigh friction, to test the sensitivity of the middle atmospheric temperature and circulation to the forcing of breaking gravity waves. It is hoped that the lessons learned here will be useful for others who are also implementing the AD parameterization in their GCMs.

The paper is organized in the following way. Section 2 describes briefly the structure of the UIUC 40-layer MST-GCM and its major difference from the UIUC 24-layer ST-GCM. The updates on the terrestrial and solar radiation modules that accommodate special needs for middle atmospheric modeling, and the corresponding changes in atmospheric heating rates, are elaborated in some detail. Section 3 describes the tests of Rayleigh friction, and weak and strong

gravity-wave forcing by the AD parameterization. Offline tests were carried out with standard atmospheric profiles to compare their forcing characteristics. Section 4 compares the middle atmospheric temperature and circulation simulated by the 40-layer MST-GCM for the three cases. The maintenance of the zonal-mean zonal winds in the middle atmosphere is examined. Section 5 presents our conclusions.

## 2. Model Description and Updates on the Radiative Transfer Modules

The 40-layer MST-GCM was developed based on the UIUC 24-layer ST GCM [Yang *et al.*, 2000]. The 24-layer ST-GCM has been used for many studies, such as the reconstruction of the radiative forcing of historical volcanic eruptions [Andronova *et al.*, 1999], simulations of climatic changes induced by the Pinatubo volcanic eruption [Yang and Schlesinger, 2002; Rozanov *et al.*, 2002] and participation in the Second Atmospheric Model Intercomparison Project [Gleckler, 1999]. It has also been coupled with the UIUC atmospheric chemical transport model (ACTM) to simulate the distributions of source gases and ozone in the stratosphere [Rozanov *et al.*, 1999a,b], and the climatic changes caused by the increase of solar UV radiation from solar minimum to solar maximum [Rozanov *et al.*, 2003].

The 40-layer MST-GCM has a horizontal resolution of  $4^\circ$  latitude by  $5^\circ$  longitude. Vertically the model extends from the earth's surface to 0.00084 hPa (about 98 km; Fig. 1). The model uses sigma ( $\sigma$ ) as its vertical coordinate, such that the earth's surface is the coordinate surface  $\sigma = 1$  and the top of the model is the coordinate surface  $\sigma = 0$ . The layers in the troposphere were prescribed and chosen to best resolve the boundary layer and the tropopause. Above the tropopause ( $\sim 120$  hPa to model top), the thickness of the layers gradually increases and follows the prescription,

$$\ln\left(\frac{P_k}{P_{k+1}}\right) / \ln\left(\frac{P_{k+1}}{P_{k+2}}\right) = 1.05, \quad (1)$$

where  $P_k$  is the pressure for the integer level  $k$  within the layer, with  $k$  increasing downward.

The 40-layer MST-GCM shares the same dynamical and physical packages as the 24-layer ST-GCM except the changes described therein. The parameterization for longwave (LW) radiative transfer of the 24-layer ST-GCM was developed by *Chou and Suarez* [1994] and modified by *Yang et al.* [2000]. It did not resolve non-local thermodynamical equilibrium (non-LTE) in the upper atmosphere. Therefore, a new module, based on the formulation of *Fomichev et al.* [1998], was developed to include in the 40-layer MST-GCM the non-LTE heating by  $\text{CO}_2$  and  $\text{O}_3$  in the upper atmosphere above 0.02 hPa. Additional absorption of solar radiation in the model atmosphere above 0.1 hPa by  $\text{O}_2$  at the Lyman-alpha line, Schumann-Runge band and Herzberg continuum was also parameterized using the *Strobel* [1978] formalism. To treat the mean-flow forcing due to breaking subgrid-scale gravity waves, the parameterization of *Palmer et al.* [1986] was included to describe topographic gravity-wave forcing in the troposphere and lower stratosphere below 10 hPa. Above 10 hPa, either Rayleigh friction or the AD parameterization was used depending upon the experimental type of this study. In addition, a momentum damping [*Hansen et al.*, 1983] was applied to both the zonal and meridional winds in the top two layers of the model. This damping acts to absorb vertically propagating waves forced from below, keeps the model from suffering computational instability, and allows larger time integration steps to be used.

To estimate the changes in heating rate due to the introduction of non-LTE parameterization, a 40-layer radiative-transfer model (RCM) extracted from the 40-layer MST-GCM was used to carry out comparative tests. The comparison was made for LW heating by CO<sub>2</sub> and O<sub>3</sub> only. Water vapor and other trace gases were not included because they are not important for non-LTE heating in the upper atmosphere. Five standard atmosphere profiles (mid-latitude summer, mid-latitude winter, sub-arctic summer, sub-arctic winter and tropics; [McClatchey *et al.*, 1972]) were tested. Figure 2 shows the heating rates between 10 hPa and the model top for the five cases. Solar heating was also included for reference. Overall, the non-LTE heating rate matches the *Chou-Suarez* LW heating rate below 0.01 hPa. Larger discrepancies are found in the upper mesosphere and lower thermosphere where both non-LTE and LTE are important. The *Chou-Suarez* parameterization largely overestimated the magnitude of the LW heating rates near the model top. Based on the RCM tests, for the layers of the MST-GCM above 0.02 hPa, the LW heating rates derived from the non-LTE routine were used to replace those from the *Chou-Suarez* parameterization. In the real atmosphere the non-LTE effect is often observed above 64 km (~0.1 hPa) [Fomichev *et al.*, 1998].

Solar radiative transfer in the 40-layer MST-GCM was adopted from *Chou and Suarez* [1999] and modified by *Yang et al.* [2000] to treat the scattering and absorption by aerosols. Absorption of solar radiation by oxygen is the primary heating source in the upper mesosphere. *Chou and Suarez* [1999] treat only the O<sub>2</sub> A and B bands (12,850-13,190 and 14,310-14,590 1/cm), and hence severely underestimated the solar heating by O<sub>2</sub> in the upper atmosphere. We added a subroutine to compute the solar absorption by O<sub>2</sub> based on *Strobel* [1978] with modifications. It computes O<sub>2</sub> absorption for the Lyman-alpha line and the Schumann-Runge band and Herzberg continuum for layers above 0.1 hPa. Figure 3 compares the solar heating

rates by O<sub>2</sub> absorption in the upper atmosphere derived from *Chou and Suarez* [1999] and the new routine for the standard atmosphere of mid-latitude summer. Starting from the middle mesosphere, the difference increases with height, and reaches ~ 6°C/day in the lower thermosphere.

### 3. Case Definition and Off-line Calculation Using Standard Atmospheric Profiles

In this study we compare three cases of mean-flow forcing due to gravity-wave breaking, one based on Rayleigh friction, and the other two from the *Alexander and Dunkerton* [1999] parameterization for strong and weak gravity-wave forcing, referred to as strong GWF and weak GWF hereinafter, respectively. These cases are defined below.

In previous studies, different types of Rayleigh friction have been used in middle atmospheric GCMs [e.g., *Boville*, 1995; *Swinbank et al.*, 1998], but they all act to damp the zonal winds with vertically varying relaxation time scales. We adopted the hyperbolic-tangent form introduced by *Holton and Wehrbein* [1980], with slight modifications gained from tuning experience that enable the 40-layer MST-GCM to simulate better the middle atmosphere circulations. The friction coefficient was determined by

$$\gamma = -\frac{1}{\alpha} \left[ 1 + \tanh\left(\frac{z-z_0}{d}\right) \right], \text{ days}^{-1}, \quad (2)$$

where  $z$  is the height of a layer in km,  $z_0$  equals 54 km in the Northern Hemisphere and 56 km in the Southern Hemisphere, and  $d = 7.5$  km. For westerly winds,  $\alpha = 3$ ; for easterly winds,  $\alpha = 15$  in the Northern Hemisphere and  $\alpha = 30$  in the Southern Hemisphere. The coefficient  $\gamma$

gradually increases with height. In the 40-layer MST-GCM, Rayleigh friction was applied only for layers above 10 hPa.

*Alexander and Dunkerton* [1999] developed a parameterization based on the convective instability criterion of *Lindzen* [1981], and assumed the momentum fluxes carried by gravity waves are all deposited locally at the level of linear wave breaking. In principle the parameterization can be used to describe mean-flow forcing due to either stationary gravity waves excited by mountains or non-stationary gravity waves from sources like convection and wind shear, or both. In any circumstance, the input of gravity-wave momentum flux needs to be specified at a level in the middle to upper troposphere. Even though there has been some estimates, the strength of this input for either stationary or non-stationary sources is still poorly constrained, primarily because of insufficient observations [*Fritts and Alexander*, 2003]. To avoid the complication of tuning the parameters related to both sources, which are all rather uncertain, we chose to keep the parameterization of *Palmer et al.* [1986] in the 40-layer MST-GCM to account for the mean-flow forcing due to topographic gravity waves in the troposphere and lower stratosphere below 10 hPa. The parameterization of *Palmer et al.* [1986] is now widely used in many climate and weather forecast models. Its use in the UIUC 24-layer ST-GCM greatly improved the model's performance [*Yang et al.*, 2000]. By doing so, we concentrate on the tuning of parameters that control the breaking and momentum deposition of non-stationary gravity waves.

For the AD scheme, there are a number of model-dependent tunable parameters that control the source of the gravity waves. Even though they have been given in *Alexander and Dunkerton* [1999], we reiterate them, along with some recommended values for non-stationary gravity waves, so the reader can understand how we have defined the strong GWF and weak

GWF cases. These parameters are: (1)  $z_0$ , the altitude of input of the gravity-wave momentum fluxes, somewhere in the upper troposphere. Usually, the higher the altitude, the larger the forcing; (2)  $c_0$  and  $\bar{c}$ , the ground-based and intrinsic phase speed at which the input momentum flux peaks. For all cases we have chosen the flux peaks at  $c_0 = 0$ ; (3)  $F_{s0}$ , a constraint on the integrated momentum fluxes crossing the tropopause, which in turn controls an intermittency factor defined in the AD scheme. The recommended value ranges from 0.001 to 0.01 Pascal. Naturally, larger  $F_{s0}$  gives stronger forcing; (4)  $B_m$ , the amplitude for the broad non-stationary source spectrum of gravity waves. The recommended value ranges from 0.1 to 1.0  $\text{m}^2/\text{s}^2$ . Usually, the larger the  $B_m$ , the smaller the forcing; (5)  $c_w$ , the half-width of the broad spectrum in phase speed. The recommended value ranges from 5 to 60 m/s. Narrower width gives smaller forcing; (6)  $L$ , horizontal wavelength, ranging from 100 to 500 km. A single number of 300 km has been used for all our cases to allow the GCM to run faster. Given the many tunable parameters, a similar distribution of forcing can be obtained by tuning when a single wavelength is used instead of multiple wavelengths; and (7)  $\Delta c$  and  $n_c$ , the spectral resolution and number of spectral points. For all our cases,  $\Delta c$  and  $n_c$  were set to 1.0 m/s and 121, respectively.

These parameters may very well vary with location and season. However, at this stage there are not sufficient observations to specify such variations. Current parameterizations of middle atmosphere gravity-wave effects all suffer acutely from the lack of constraints on wave sources and tunable parameters [Fritts and Alexander, 2003]. We tested first the AD scheme by prescribing globally uniform parameters – our weak GWF case, and then by varying somewhat these parameters in space – our strong GWF case. For each case, different combinations of parameters were explored to find the best solution. For results reported here, for the weak GWF

case,  $z_0 = 470$  hPa,  $F_{s0} = 0.006$ ,  $B_m = 0.4$ , and  $c_w = 40$  at all model grid points. For the strong GWF case,  $z_0 = 470$  hPa at all model grid points; and if the zonal wind in the middle mesosphere is easterly,  $F_{s0} = 0.015$ ,  $B_m = 0.3$ , and  $c_w = 10$ , and if the zonal wind is westerly,  $F_{s0} = 0.04$ ;  $B_m = 0.45$ ; and  $c_w = 25$ . For the strong GWF case, after the forcing is computed it is further scaled by a factor at all latitudes for layers above 0.04 hPa. The factor is defined as  $0.04/P(k)$ , where  $P(k)$  is model layer pressure in hPa. We found this scaling is necessary for the UIUC 40-layer MST-GCM if the wind reversal near the mesopause in the summer hemisphere is to be simulated.

To gain a general understating of the characters of Rayleigh friction and the AD parameterization, we compare off-line gravity-wave forcing for the three cases using the COSPAR International Reference Atmosphere (CIRA-86) [Fleming *et al.*, 1988, 1990]. The dataset contains monthly mean zonal-mean temperature, zonal wind and geopotential height in  $5^\circ$  interval covering the latitudes from  $80^\circ\text{S}$  to  $80^\circ\text{N}$ , and in 0.25 log-pressure interval extending from 1013.0 hPa to 0.0000254 hPa ( $\sim 120$  km). The tests performed here used COSPAR data up to 0.00084 hPa (the top layer of the 40-layer MST-GCM). Figure 4 shows zonal wind accelerations in m/s/day in January and July for the cases of Rayleigh friction, and the weak and strong GWF, respectively.

For Rayleigh friction, the forcing always acts to damp the mean flow, is proportional to the strength of the mean flow at a given altitude, and exists at all time and in all places where the scheme is applied. In general, large forcing is found adjacent to the cores of middle atmosphere jets. The largest forcing reaches  $-25$  m/s/day for westerly winds and 5 m/s/day for easterly winds in the middle mesosphere. For the AD parameterization, unlike Rayleigh friction, the forcing

tends to accelerate the mean flow in the middle to lower stratosphere and to decelerate the mean flow in the upper mesosphere, and is not ubiquitous since gravity waves break only under certain circumstances. (Note that large amplitude mountain waves with phase speed close to zero tend to decelerate the mean flow at all levels [*Fritts and Alexander, 2003*].) For the weak GWF case, the largest forcing is found in the middle mesosphere close to the middle atmosphere jet cores, with a magnitude that reaches 50 m/s/day for both westerly and easterly winds. All momentum is deposited below the mesopause. For the strong GWF case, however, the largest forcing does not coincide with the middle atmosphere jets. The waves break at a much higher altitude, especially in the summer atmosphere. The forcing is greater than 100 m/s/day (200 m/s/day) in January (July) in the upper mesosphere and lower thermosphere above the middle atmosphere easterly jets. This large forcing is found to be necessary for the MST-GCM to simulate the wind reversal near the mesopause, as explained in the next section.

#### 4. MST-GCM Simulation Results

Three experiments were carried out with the UIUC 40-layer MST-GCM for the cases described in section 3 to test the sensitivity of the middle atmosphere temperature and circulation to the mean-flow forcing by gravity-wave breaking. Each experiment was run for ten years starting from the same initial condition. For lower boundary conditions, sea-surface temperature and sea ice were prescribed to be the AMIP-II (Atmospheric Modeling Intercomparison Project) monthly means, which are the averages from 1979 through 1996 [*Gleckler, 1999*], and were updated daily by interpolation between consecutive monthly values. The initial condition was derived from the 1979-95 climatology of the NCEP/NCAR reanalysis [*Kalnay et al., 1996*] for the model atmosphere from the earth's surface to 10 hPa, and from the COSPAR International

Reference Atmosphere (CIRA-86) [Fleming *et al.*, 1988, 1990] for the model atmosphere above. Data from the 24-layer ST-GCM restart file were used for variables that are not available from observations. For each case the model was run for 10 years. Results from the last 8 years of simulation are used for the following analysis.

1) *Zonal Mean Temperature and Circulation*

Latitude–height cross–sections of the simulated monthly mean zonal–mean zonal winds are presented in Fig. 5 for January and July, together with the corresponding observations. In the troposphere and lower stratosphere, the simulated zonal winds are quite similar to each other for the three cases in both months, probably because the Palmer *et al.* [1986] topographic gravity-wave drag parameterization was applied in each case. The strength and location of the observed troposphere jets are all well captured. Compared to the UIUC 24-layer ST-GCM [Yang *et al.*, 2000], this 40-layer GCM greatly improved the simulation of the stratospheric polar-night jet in both hemispheres. In the 24-layer GCM, the simulated wintertime polar-night jet in each hemisphere was too weak and was shifted equatorward of its observed position. This improvement was attributed mostly to the much higher model top in the 40-layer GCM [Yang, 2000]. In the middle atmosphere, for all cases and in both months the simulated jet cores of westerly wind are located about 5 to 10 degrees too close to the poles and at a lower altitude than the observed. As for many other mesospheric GCMs [e.g., Boville, 1995; Beagley *et al.*, 1997; Manzini and McFarlane, 1998], the observed equatorward tilt of the jet core from about the stratopause to the mesopause is not captured. Overall, the simulation for the case of strong GWF compares most favorably with observations in terms of the strength and location of middle atmosphere westerly winds.

For the summer-hemisphere easterly winds, the observed tilt of the jet core from the tropical upper stratosphere to the polar upper mesosphere was simulated for all the three cases, but the strength of the easterly jet varies considerably. It is extremely weak for the case of weak GWF (Figs. 5c and 5g). It compares more favorably with the CIRA data for the cases of Rayleigh friction and strong GWF, though for the former it is slightly weaker and for the latter it is slightly stronger than the observed. A comparison between Fig. 4 and Fig. 5 implies that to simulate the observed jet core of easterly winds in the middle mesosphere requires only a small gravity-wave forcing. In Fig. 4 the forcing for the case of weak GWF reached 50 m/s near 0.1 hPa in the middle latitudes, while it is only a few meters per second for the other two cases.

The most appealing feature for the case of strong GWF is that the observed wind reversal is simulated in the summer hemisphere from easterly to westerly crossing the mesopause (Figs. 5d and 5h). This is a result of the strong eastward wind accelerations in the upper mesosphere and lower thermosphere due to gravity-wave breaking, which was tuned based on the AD parameterization for this purpose (Figs. 4c and 4f). We learned that with Rayleigh friction it was impossible to capture this reversal no matter how we tuned the parameters, since Rayleigh friction acts only to damp the mean flow. It still presents a big challenge for many middle atmospheric GCMs to simulate this wind reversal [e.g., *Medvedev et al.*, 1998]. Although it is the result of parameter tuning that leads to the improved simulation of the middle atmospheric winds, this exercise also enables the model to simulate better the middle atmospheric temperatures (see the following subsection).

Figure 6 presents the observed zonal-mean temperatures in January and July, and the differences between the model simulations and observations. In both January and July for all cases, the model generally simulates well the temperatures in the troposphere and stratosphere

everywhere except in the lower polar stratosphere over the South Pole. Temperature biases are less than a few degrees in the troposphere and about 10°C in the stratosphere in middle to low latitudes. At the South Pole, the temperature in the lower stratosphere is about 20°C colder than the observed. From numerical experiments with the ECHAM-5 GCM presented by E. Roeckner (2003, personal communications), this lower stratosphere cold bias results from low model resolution in the vertical direction.

In the mesosphere and lower thermosphere, for the cases of Rayleigh friction and weak GWF, the model failed to simulate the cold polar mesopause in the summer hemisphere. Near the model's top, large warm biases of up to 60°C are found in the southern high latitudes in January (Figs. 6b and 6c) and in the northern high latitudes in July (Figs. 6f and 6g). For the case of strong GWF, the warm bias was almost eliminated, and even a slightly cold bias built up. This cold mesopause in the summer hemisphere is closely linked to the reversal of zonal winds from easterly below the mesopause to westerly winds above. It has been known for a long time that, in the mesosphere and lower thermosphere, the mean-flow forcing due to gravity-wave breaking causes the reversal of zonal-mean winds, drives a mean meridional transport circulation, and leads to a warm winter mesopause and a cold summer mesopause (see the review by *Holton and Alexander* [2000] and references therein). In the next section we compare how the transport circulations differ among the three experiments, and how the mean flow is maintained in the atmosphere.

## 2) *Residual Circulation and Maintenance of the Zonal-Mean Zonal Winds in the Middle Atmosphere*

To compare the mean–meridional circulations between the three experiments from a Lagrangian point of view, we computed the residual meridional and vertical winds from the framework of the transformed Eulerian-mean circulation [Andrews and McIntyre, 1976]. Formally, the residual circulation is the part of the mean meridional circulation that is not balanced by the convergence of model-resolved eddy enthalpy fluxes. The calculation was performed using the eddy fluxes of momentum and potential temperature sampled at 6-hour intervals and the monthly means of other quantities on isobaric surfaces. For each case, the monthly mean residual circulation for individual years was computed before the multi-year averages were derived.

Figure 7 presents the 8-year averaged residual meridional wind  $[\bar{v}]_r$  and residual vertical wind  $[\bar{w}]_r$  from 900 hPa to 0.0014 hPa for the three cases in July. Results for January are not shown, as they are similar to those for July. In computing, the approximation  $[\bar{\omega}]_r = -[\bar{\rho}]g[\bar{w}]_r$  was assumed to convert  $[\bar{\omega}]_r$  in Pascal/s in p-coordinate to  $[\bar{w}]_r$  in cm/s in z-coordinate, where  $[\bar{\rho}]$  is the monthly mean zonal–mean air density. For all cases,  $[\bar{v}]_r$  is negative in Fig. 7 in the middle mesosphere, indicating a pole-to-pole southward transport in July. Air ascends in the summer mesosphere ( $[\bar{w}]_r > 0$ ) and descends in the winter mesosphere ( $[\bar{w}]_r < 0$ ). The weakest residual circulation is found for the case of weak GWF. The most vigorous residual circulation is found for the case of strong GWF, in which  $[\bar{v}]_r$  reaches about  $-8$  m/s near the mesopause in the northern middle and high latitudes, and  $[\bar{w}]_r$  reaches  $\sim 3$  cm/s in the middle and upper mesosphere near the North Pole. This strong ascending motion leads to a stronger adiabatic cooling; therefore, the warm bias found for the cases of Rayleigh friction and weak GWF disappeared for the case of strong GWF. Some global and mechanistic model studies suggest

that to account for the summer mesopause thermal structure  $[\bar{v}]_r$  and  $[\bar{w}]_r$  need to reach ~20-30 m/s and 5 cm/s, respectively (for a review see *Fritts and Alexander*, [2003]).

To understand why strong forcing of gravity-wave breaking is required to sustain the thermal structure in the middle atmosphere, we consider further how the zonal-mean flow is maintained in the atmosphere for the case of strong GWF. In the spherical pressure coordinate system and in the framework of transformed Eulerian mean circulation, the tendency of the zonal-mean zonal wind can be written as [Piexóto and Oort, 1992],

$$\frac{\partial[u]}{\partial t} = f[\bar{v}]_r + \frac{1}{R\cos\phi} \text{div}\bar{F} + [F_\lambda], \quad (3)$$

where  $\text{div}\bar{F}$  is the divergence of the Eliassen-Palm (EP) flux,  $[F_\lambda]$  represents the frictional force near the earth's surface, and, for GCMs, any parameterized forces that are not explicitly resolved by the model's dynamical processes, including those due to gravity-wave breaking, sponge-layer friction, diffusion and convection. The strength of the EP flux measures the interaction between the mean flow and eddy disturbances, and the divergence of EP flux reflects the momentum forcing due to model-resolved eddies that interact with the mean flow. For a long-term mean,  $\partial[u]/\partial t \rightarrow 0$ , hence the three terms on the right-hand side of Eq. (3) should be in balance.

Figs. 8a and 8b depict the derived 8-year mean EP-flux divergence ( $\text{div}\bar{F}/R\cos\phi$ ) in July for the case of strong GWF, and the forcing on the mean flow due to the meridional residual winds ( $f[\bar{v}]_r$ ). To obtain  $[F_\lambda]$ , we accumulated the changes in the zonal-mean zonal wind due to the different forcings that are not explicitly resolved by the GCM but are instead parameterized, at each time step during model integration and saved the output of monthly means. Shown in

Figs. 8c and 8d are the zonal-mean tendencies of the zonal wind in July contributed by the breaking of non-topographic gravity waves (the AD parameterization, Fig. 8c), and by the breaking of topographic gravity waves [Palmer *et al.*, 1986], which was applied only to the model layers below 10 hPa, together with the damping effect of the sponge-layer friction, which was applied to the top two model layers (Fig. 8d). Other types of parameterized forcing on the mean flow, such as surface friction and convection, are ignored because they are either confined to the planetary boundary layer or are relatively unimportant. For all plots in Fig. 8, the forcing has been converted to tendencies of the zonal wind in m/s/day.

Examination of Figure 8 suggests that, in the middle atmosphere, the zonal-mean zonal wind is primarily maintained by a balance between the Coriolis force associated with the meridional transport circulation (Fig. 8b) and the parameterized forcing due to the breaking of subgrid-scale gravity waves (Fig. 8c). The contribution by the model-resolved eddy disturbances, expressed as the divergence of the EP fluxes (Fig. 8a), is secondary. For example, in the southern high latitudes near the mesopause the deceleration of the mesospheric westerly jets in July by the breaking of gravity waves reaches  $\sim 40$  m/s/d, while the deceleration by the EP-flux divergence is only about  $\sim 10$  m/s. In the northern high latitudes near the mesopause the forcing of the zonal winds by the meridional transport circulation is almost entirely balanced by the forcing due to gravity-wave breaking, with minor contributions from the sponge-layer friction. The forcing by gravity-wave breaking in the northern mesosphere is much larger than in the southern mesosphere.

The situation in the troposphere is completely different from that in the mesosphere. The balance is achieved primarily between the forcing due to the transport circulation (Fig. 8b) and the model-resolved eddy disturbances, that is, the EP-flux divergence (Fig. 8a). Compared to the

EP-flux divergence (Fig. 8a), the forcing due to the breaking of both non-stationary (Fig. 8c) and stationary (Fig. 8d) gravity waves is negligible. In the lower and middle stratosphere, all forcing terms in Eq. (3) are much smaller than in the mesosphere and troposphere. The forcing due to topographic gravity-wave breaking (Fig. 8d) decelerates the westerly winds in the southern stratosphere, and the forcing due to non-stationary gravity-wave breaking (Fig. 8c) accelerates the easterly winds in the northern stratosphere. The magnitude reached about 1.0 m/s/day in both hemispheres. The sign and magnitude are consistent with some simple model estimates [Alexander and Rosenlof, 1996; Ray *et al.*, 1998].

The above analysis infers that in the mesosphere and lower thermosphere, strong forcing due to gravity-wave breaking is required to maintain the observed mean flow, to excite the strong meridional pole-to-pole transport circulation, and to enable the GCM to simulate the observed cold summer mesopause. This is especially true in the summer mesosphere where the forcing due to the model-resolved eddy disturbances is much weaker than in the winter mesosphere.

### 3) *Equatorial Zonal Winds*

The quasi-biennial oscillation (QBO) and the semi-annual oscillation (SAO) are the most intriguing features of the observed tropical atmospheric circulation. We examine how they are simulated by the UIUC MST-GCM for the three cases of gravity-wave parameterization. Figure 9 presents monthly mean zonal-mean zonal winds at the equator from 100 hPa to the top of the model. For the case of Rayleigh friction, the model failed to capture the SAO in the mesosphere and upper stratosphere. Easterly winds persist all the time. There is no downward phase propagation. For the cases of weak and strong GWF, the model was able to produce strong SAOs. Both the easterly and westerly phases have prominent downward-phase propagation

similar to the observations. However, the model failed to simulate the QBO in both of the cases. Although the AD parameterization proves to be superior to Rayleigh friction in many aspects, it may still require more careful tuning, if possible at all, to simulate the QBO. Inferring from the studies by *Takahashi and Shiobara* [1995] and *Takahashi* [1999], probably with a much higher vertical resolution the UIUC MST-GCM would simulate the QBO, no matter what kind of parameterization for gravity-wave breaking was used.

## 5. Summary and Discussion

To study the impact of solar variability on atmospheric chemical composition and climate, a 40-layer GCM extending up to about 100 km has been developed at the University of Illinois at Urbana-Champaign based on the UIUC 24-layer ST-GCM [*Yang et al.*, 2000]. Efforts have been made to simulate better the temperature and circulation of the middle atmosphere because of their great impact on middle atmospheric chemical reactions and transport. In addition to the updates of the solar and longwave radiative transfer routines, attention has been paid to a better representation of the forcing on mean flow due to gravity-wave breaking in the middle atmosphere. In this paper we have documented the sensitivity of the middle atmospheric temperature and circulation in the UIUC 40-layer MST-GCM to the treatment of subgrid-scale gravity-wave forcing. Three sensitivity experiments were performed. The forcing due to the breaking of non-stationary gravity waves in the middle atmosphere was represented first by Rayleigh friction, and then by the parameterization of *Alexander and Dunkerton* [1999], separately with weak and strong breaking effects. In all experiments the *Palmer et al.* [1986] parameterization was included to treat the breaking of topographic gravity waves in the troposphere and lower stratosphere.

Results showed that for the cases of Rayleigh friction and weak GWF, the GCM was not able to simulate the observed reversal of the zonal winds from easterly to westerly in the summer mesosphere near the mesopause. The meridional transport circulation was too weak, hence the adiabatic cooling in the summertime upper mesosphere and lower thermosphere was insufficient to produce the observed cold mesopause. Consequently, large warm biases of up to 60°C occurred near the summer mesopause. For the case of strong GWF, in which the forcing due to gravity-wave breaking reached more than 100 m/s/day near the summer mesopause, the GCM produced a much stronger meridional transport circulation than for the other two cases. As a result the model was able to capture the observed wind reversal, and essentially eliminated the warm biases. With the AD parameterization, the model was also able to simulate much more realistically the SAO in the upper atmosphere.

Budget analysis indicates that, for the UIUC 40-layer MST-GCM, the zonal-mean zonal wind in the middle atmosphere is primarily maintained by the balance between the Coriolis force associated with the meridional transport circulation and the parameterized gravity-wave forcing. The contribution by the model-resolved wave-mean interaction in terms of EP-flux divergence was secondary. The situation in the troposphere is totally different. The balance was achieved primarily by the forcing due to transport circulation and EP-flux divergence. In the upper troposphere and lower stratosphere, stationary (topographic) gravity waves act to slow down westerly winds and non-stationary gravity waves act to accelerate easterly winds, with the forcing magnitude both reached only ~1.0 m/s/day.

These results imply that in the mesosphere and lower thermosphere, strong forcing due to gravity-wave breaking is required to maintain the observed mean flow, to excite the strong meridional pole-to-pole transport circulation, and to simulate the reversed pole-to-pole

temperature gradient near the mesopause. *Norton and Thuburn* [1999] also found similar sensitivity of the mesospheric circulation and temperature to the strength of gravity-wave forcing in the Extended UGAMP GCM, which uses a modified version of *Palmer et al.* [1986] gravity-wave scheme to account for the subgrid-scale gravity-wave forcing through the atmosphere.

Even though in recent years considerable advances have been made in both the observation and theoretical understanding of middle atmospheric gravity waves [*Fritts and Alexander*, 2003], parameterization schemes suitable for their use in middle atmospheric GCMs are still in the developing stage. Almost all current schemes [e.g., *Medvedev and Klaasen*, 1995; *Hines*, 1997a, b; *Alexander and Dunkerton*, 1999; *Warner and McIntyre*, 2001] need a set of predetermined parameters that are not well constrained by observations; therefore, extensive tuning is unavoidable. The properties of the input parameters for the AD scheme that we inferred in this study from the constraint of the simulated circulation and temperature are not unique, and definitely are model dependent. Although we have been able to improve our model's performance in many aspects by carefully choosing the parameters, further advances still depend critically on more accurate parameterization of gravity-wave breaking throughout the atmosphere.

**Acknowledgments.** This material is based upon work supported by the National Aeronautics and Space Administration under Award No. NAG5-10942. Any opinions, findings, and conclusions or recommendations expressed in this publication are those of the authors and do not necessarily reflect the views of the National Aeronautics and Space Administration. The authors

thank M. Joan Alexander for providing us the code for gravity-wave forcing parameterization.

F.Y. is grateful to William K. M. Lau for his encouragement.

## REFERENCES

- Alexander, M. J., and T. J. Dunkerton, A spectral parameterization of mean-flow forcing due to breaking gravity waves, *J. Atmos. Sci.*, *56*, 4167–4182, 1999.
- Alexander, M. J., and K. H. Rosenlof, Nonstationary gravity wave forcing of the stratospheric zonal mean wind, *J. Geophys. Res.*, *101*, 23,465–23,474, 1996.
- Andrews, D.G., and M.E. McIntyre, Planetary waves in horizontal and vertical shear: The generalized Eliassen-Palm relation and the mean zonal acceleration, *J. Atmos. Sci.*, *33*, 2031–2048, 1976.
- Andronova, N. G., E. Rozanov, F. Yang, M. E. Schlesinger, and G. L. Stenchikov, Radiative forcing by volcanic aerosols from 1850 through 1994, *J. Geophys. Res.*, *104*, 16 807–16 826, 1999.
- Beagley, S. R., J. D. Grandpre, J. N. Koshyk, N. A. McFarlane, and T. G. Shepherd, Radiative-dynamical climatology of the first-generation Canadian middle atmosphere model, *Atmosphere–Ocean*, *35*, 293–331, 1997.
- Boville, B. A., Middle atmosphere version of CCM2 (MACCM2): Annual cycle and interannual variability, *J. Geophys. Res.*, *100*, 9017–9039, 1995.
- Chou, M. D., and M. J. Suarez, An efficient thermal infrared radiation parameterization for use in General Circulation Models, Technical Report Series on Global Modeling and Data Assimilation, National Aeronautical and Space Administration/TM–1994–104606, 3, 85 pp, 1994.
- Chou, M. D., and M. J. Suarez, A solar radiation parameterization for atmospheric studies, Technical Report Series on Global Modeling and Data Assimilation, National Aeronautical and Space Administration/TM–1999–104606, 15, 40 pp, 1999.

- Fleming, E.L., S. Chandra, M.R. Schoeberl, and J.J. Barnett, Monthly mean global climatology of temperature, wind, geopotential height, and pressure for 0-120 km, NASA Tech. Memo. NASA TM-100697, 85 pp, 1988.
- Fleming, E.L., S. Chandra, J.J. Barnett, and M. Corney, Zonal mean temperature, pressure, zonal wind, and geopotential height as functions of latitude, COSPAR International Reference Atmosphere:1986, Part II: Middle Atmosphere Models, *Adv. Space Res.*, Vol. 10, No. 12, pp. 11-59, 1990.
- Fomichev, V. I., J.-P. Blanchet, and D. S. Tuner, Matrix parameterization of the 15 micro CO<sub>2</sub> band cooling in the middle and upper atmosphere for variable CO<sub>2</sub> concentration, *J. Geophys. Res.*, 103, 11,505-11,528, 1998.
- Fritts, D. C., and M. J. Alexander, Gravity wave dynamics and effects in the middle atmosphere, *Rev. Geophys.*, 41(1), 1003, doi:10.1029/2001RG000106, 2003.
- Fritts, D. C., and W. Lu, Spectral estimates of gravity wave energy and momentum fluxes, II, Parameterization of wave forcing and variability, *J. Atmos. Sci.*, 50, 3695-3713, 1993.
- Gleckler, P., AMIP Newsletter, No. 9. WNGE Atmospheric Model Intercomparison Project, Livermore, 8 pp, 1999.
- Hamilton, K. (Ed.), *Gravity Wave Processes and Their Parameterization in Global Climate Models*, 404 pp., Springer-Verlag, New York, 1997.
- Hansen, J. A., G. Russell, D. Rind, P. Stone, A. Lacis, S. Lebedeff, R. Ruedy, and L. Travis, Efficient three-dimensional global models for climate studies: Models I and II. *Mon. Wea. Rev.*, 111, 609-662, 1983.
- Hines, C. O., Doppler-spread parameterization of gravity-wave momentum deposition in the middle atmosphere, 1, Basic formulation, *J. Atmos. Sol. Terr. Phys.*, 59, 371-386, 1997a.

- Hines, C. O., Doppler-spread parameterization of gravity-wave momentum deposition in the middle atmosphere, 2, Broad and quasi monochromatic spectra, and implementation, *J. Atmos. Sol. Terr. Phys.*, 59, 387–400, 1997b.
- Holton, J. R., and M. J. Alexander, The role of waves in the transport circulation of the middle atmosphere, in *Atmospheric Science Across the Stratopause, Geophys. Monogr. Ser.*, vol. 123, edited by D. E. Siskind, S. D. Eckermann, and M. E. Summers, pp. 21–35, AGU, Washington, D. C., 2000.
- Holton, J. R., and W. M. Wehrbein, A numerical model of the zonal mean circulation of the middle atmosphere, *Pure Appl. Geophys.*, 118, 284–306, 1980.
- Kalnay, E., K. M. R. Kistler, W. Collins, D. Deaven, L. Gandin, M. Iredell, S. Saha, G. White, J. Woollen, Y. Zhu, A. Leetmaa, R. Reynolds, M. Chelliah, W. Ebisuzaki, W. Higgins, J. Janowiak, K. C. Mo, C. Ropelewski, J. Wang, R. Jenn, and D. Joseph, The NCEP/NCAR 40-year reanalysis project, *Bull. Amer. Meteor. Soc.*, 77, 437–471, 1996.
- Langematz, U., and S. Pawson, The Berlin troposphere–stratosphere–mesosphere GCM: Climatology and forcing mechanism. *Quart. J. Roy. Meteor. Soc.*, 123, 1075–1096, 1997.
- Lindzen, R. S., Turbulence and stress owing to gravity wave and tidal breakdown. *J. Geophys. Res.*, 86, 9709–9714, 1981.
- Lott, F., and M. J. Miller, A new subgrid-scale orographic drag parameterization: Its formulation and testing, *Q. J. R. Meteorol. Soc.*, 123, 101–127, 1997.
- Manzini E., and L. Bengtsson, Stratospheric climate and variability from a general circulation model and observations, *Clim. Dyn.*, 12, 615–639, 1996.

- Manzini, E., and N. A. McFarlane, The effect of varying the source spectrum of a gravity wave parameterization in a middle atmosphere general circulation model, *J. Geophys. Res.*, *103*, 31,523–31,539, 1998.
- McClatchey, R. A., R. W. Fenn, J. E. A. Selby, F. E. Volz, and J. S. Garing, Optical Properties of the Atmosphere, Air Force Cambridge Research Laboratories, AFCRL-72-0497, 221 pp, 1972.
- McFarlane, N. A., The effect of orographically excited gravity wave drag on the general circulation of the lower stratosphere and troposphere, *J. Atmos. Sci.*, *44*, 1775–1800, 1987.
- Medvedev, A. S., and G. P. Klaassen, Vertical evolution of gravity wave spectra and the parameterization of associated wave drag, *J. Geophys. Res.*, *100*, 25,841–25,853, 1995.
- Medvedev, A. S., G. P. Klaassen, and S. R. Beagley, On the role of an anisotropic gravity wave spectrum in maintaining the circulation of the middle atmosphere, *Geophys. Res. Lett.*, *25*, 509–512, 1998.
- Norton, W. A.; and J. Thuburn, Sensitivity of mesospheric mean flow, planetary waves, and tides to strength of gravity wave drag, *J. Geophys. Res.*, *104*, 30,897–30,912, 1999.
- Palmer, T. N., G. J. Shutts, and R. Swinbank, Alleviation of a systematic westerly bias in general circulation and numerical weather prediction models through an orographic gravity wave drag parameterization, *Quart. J. Roy. Meteor. Soc.*, *112*, 1001–1039, 1986.
- Piexóto, J. P., and A. H. Oort, *Physics of Climate*, American Physical Society (New York), 520 pp, 1992.
- Ray, E. A., M. J. Alexander, and J. R. Holton, An analysis of the structure and forcing of the equatorial semiannual oscillation in zonal wind, *J. Geophys. Res.*, *103*, 1759–1774, 1998.

- Rozanov, E., V. Zubov, M. Schlesinger, F. Yang, and N. Andronova, Three-dimensional simulations of ozone in the stratosphere and comparison with UARS data, *Physics and Chemistry of the Earth*, 24, 459-463, 1999a.
- Rozanov, E., V. Zubov, M. Schlesinger, F. Yang, and N. Andronova, The UIUC 3-D Stratospheric Chemical Transport Model: Description and Evaluation of the Simulated Source Gases and Ozone, *J. Geophys. Res.*, 104, 11 755–11 781, 1999b.
- Rozanov, E. V., M. E. Schlesinger, N. G. Andronova, F. Yang, S. L. Malyshev, V. A. Zubov, T. A. Egorova, and B. Li, Climate/chemistry effects of the Pinatubo volcanic eruption simulated by the UIUC stratosphere/troposphere GCM with interactive photochemistry, *J. Geophys. Res.*, 107 (D21), 4594, doi:10.1029/2001JD000974, 2002.
- Rozanov, E. V., M. E. Schlesinger, T. A. Egorova, B. Li, N. Andronova, and V.A. Zubov, Atmospheric Response to the Observed Increase of Solar UV Radiation from Solar Minimum to Solar Maximum Simulated by the UIUC Climate-Chemistry Model, *J. Geophys. Res.*, 2003 (submitted).
- Strobel, D. F., Parameterization of the atmospheric heating rate from 15 to 120 km due to O<sub>2</sub> and O<sub>3</sub> absorption of solar radiation, *J. Geophys. Res.*, 83, 6225-6230, 1978.
- Swinbank, R., W. A. Lahoz, A. O'Neill, C. S. Douglas, A. Heaps, and D. Podd, Middle atmosphere variability in the UK Meteorological Office Unified Model, *Quart. J. Roy. Meteor. Soc.*, 124, 1485–1526, 1998.
- Takahashi, M., Simulation of the quasi-biennial oscillation in a general circulation model, *Geophys. Res. Lett.*, 26, 1307–1310, 1999.
- Takahashi, M., and M. Shiobara, A note on a QBO-like oscillation in the 1/5 sector CCSR/NIES GCM, *J. Meteor. Soc. Japan*, 73, 131–137, 1995.

- Warner, C. D., and M. E. McIntyre, An ultra-simple spectral parameterization for non-orographic gravity waves, *J. Atmos. Sci.*, 58, 1837–1857, 2001.
- Yang, F., Radiative forcing and climatic impact of the Mount Pinatubo volcanic eruption, Ph.D. Dissertation, University of Illinois at Urbana-Champaign, pp 219, 2000.
- Yang, F., and M. E. Schlesinger, On the surface and atmospheric temperature changes following the 1991 Pinatubo volcanic eruption: A GCM study, *J. Geophys. Res.*, 107(D8), 4073, doi:10.1029/2001JD000373, 2002.
- Yang, F., M. E. Schlesinger, and E. Rozanov, Description and performance of the UIUC 24-layer stratosphere/troposphere general circulation model, *J. Geophys. Res.*, 105 (D14), 17,925-17,954, 2000.

## Figure Captions

**Fig. 1.** Vertical structure of the UIUC 40-layer MST-GCM.

**Fig. 2.** Long-wave (LW) heating rates computed by a 40-layer radiative-transfer model with the non-LTE code and Chou-Suarez code, respectively, for five standard atmospheric profiles. Solar heating (SW) was also included for reference. Only CO<sub>2</sub> and O<sub>3</sub> were included in the radiative transfer calculation.

**Fig. 3.** Solar heating rates by O<sub>2</sub> computed with the module of *Chou and Suarez* [1999] and a modified module of *Strobel* [1978] for the case of mid-latitude summer atmosphere.

**Fig. 4.** Mean-flow forcing (color shadings edged by thick green lines) of zonal-mean zonal winds (m/s/day) due to breaking of gravity waves in January (left panels) and July (right panels), for the cases of Rayleigh friction (top panels), weak GWF (middle panels), and strong GWF (bottom panels). For reference, the background zonal-mean zonal winds are plotted as black contours with a 10 m/s interval. Dotted lines are for easterly winds, and unbroken lines for westerly winds. The zero contour line is omitted.

**Fig. 5.** Zonal-mean zonal wind in January (left panels) and July (right panels) for observations (a and e), and for simulations by the UIUC 40-layer MST-GCM for the cases of Rayleigh friction (b and f), weak GWF (c and g), and strong GWF (d and h). The observations consist of NCEP/NCAR Reanalysis averaged for the 1979-1995 period below 10 hPa and CIRA-86 data

above. All simulation results are 8-year averages. The contour interval is 10 m/s. Easterly winds are shaded.

**Fig. 6.** Zonal-mean temperatures for observations (a and e), and the differences from observations of the zonal-mean temperatures simulated by the UIUC 40-layer MST-GCM for the cases of Rayleigh friction (b and f), weak GWF (c and g), and strong GWF (d and h). The observations consist of NCEP/NCAR Reanalysis averaged for the 1979-1995 period below 10 hPa and CIRA-86 data above. All simulation results are 8-year averages. The contour interval is 10°C. Shadings indicate warm biases for simulations and above-zero temperature for observations. All plots in the left-hand panels are for January and in the right-hand panels for July.

**Fig. 7.** Residual meridional wind (left panels) and residual vertical wind (right panels) in July for the cases of Rayleigh friction (a and d), weak GWF (b and e), and strong GWF (c and f). For the meridional wind, the contour interval is 1.0 m/s with  $\pm 0.5$  m/s lines added. Negative values indicate southward motion. For the vertical wind, the contour interval is 1.0 cm/s with  $\pm 0.5$  cm/s lines added. Negative values indicate downward motion.

**Fig. 8.** Accelerations of the zonal-mean zonal wind in July for the case of strong GWF due to (a) EP-flux divergence, (b) residual meridional wind, (c) the breaking of non-stationary gravity waves from the AD parameterization, and (d) the breaking of topographic gravity waves from the Palmer *et al.* [1986] parameterization, which was applied only below 10 hPa, and the “sponge-layer” friction, which was applied to the top two layers of the model. Above 10 hPa, the contour

interval is 10 m/s/day. Below 10 hPa, the contour interval is 3 m/s/day in (a) and (b), with the  $\pm 1$  and  $\pm 2$  contours added, and 1 m/s/day in (c) and (d). Negative values indicate westward wind acceleration.

**Fig. 9.** Monthly zonal-mean zonal winds at the equator for the cases of (a) Rayleigh friction, (b) weak GWF, and (c) strong GWF. The contour interval is 10 m/s. Easterly winds are shaded.

### VERTICAL COORDINATE FOR UIUC MST-GCM

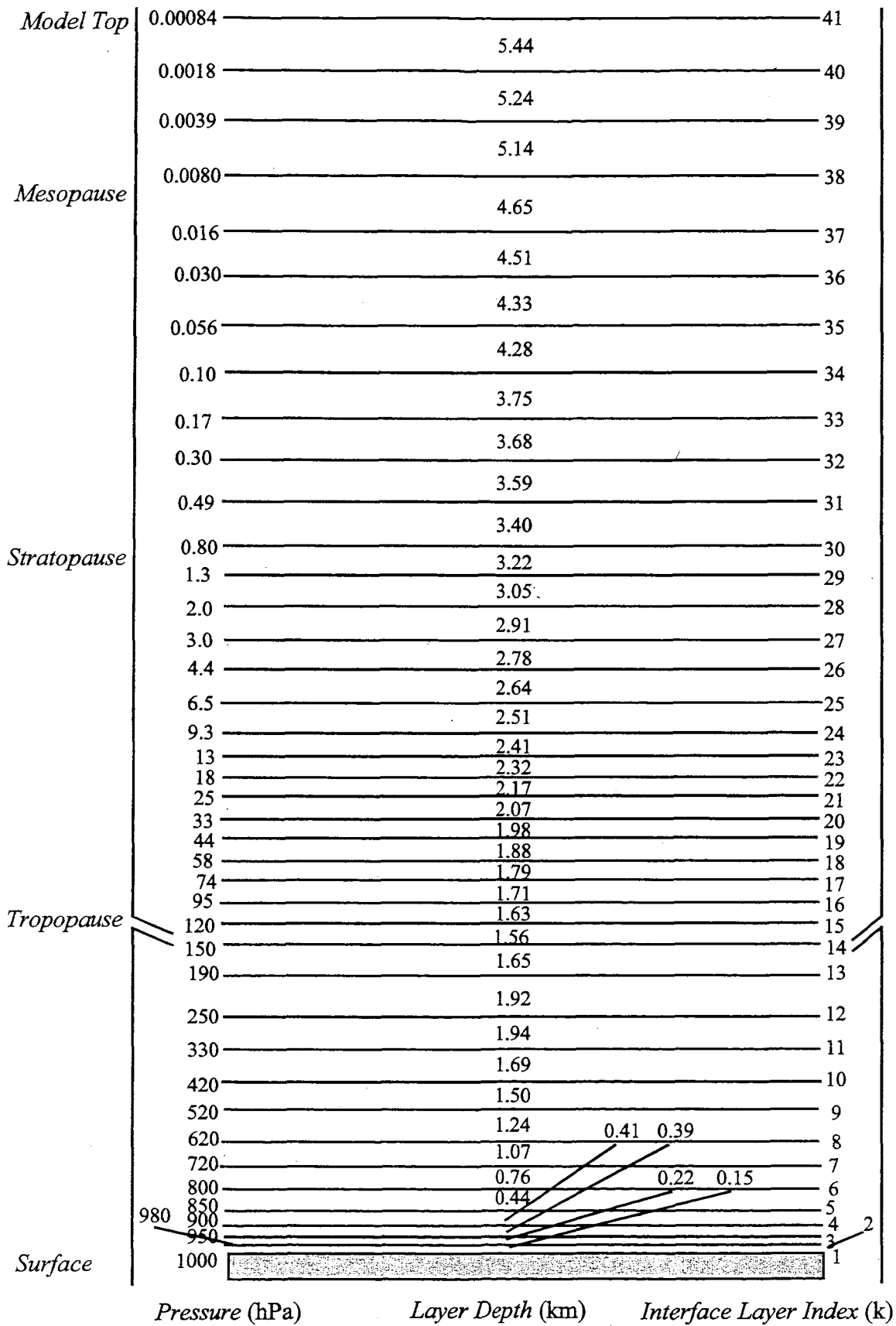


Fig.1

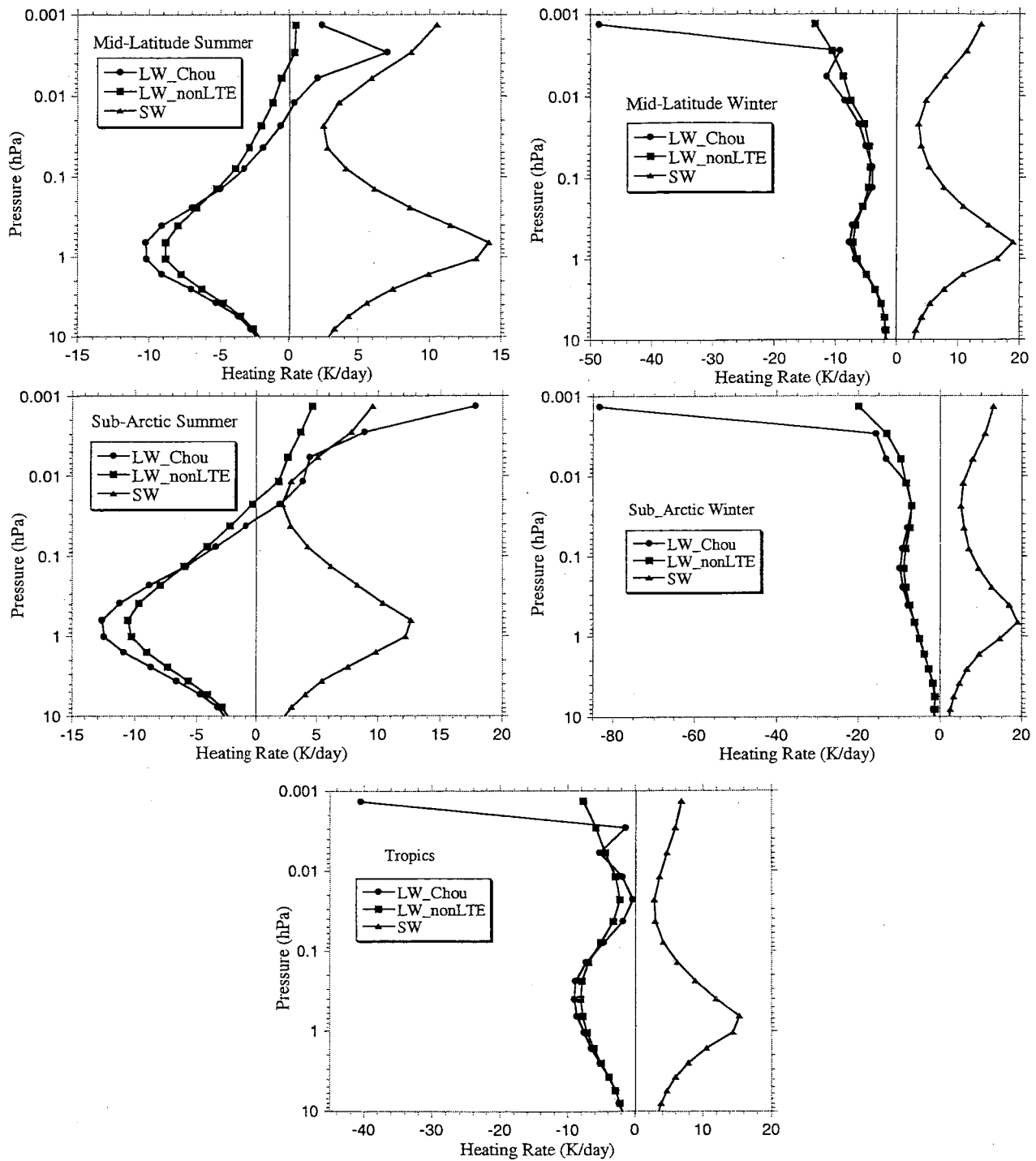


Fig.2

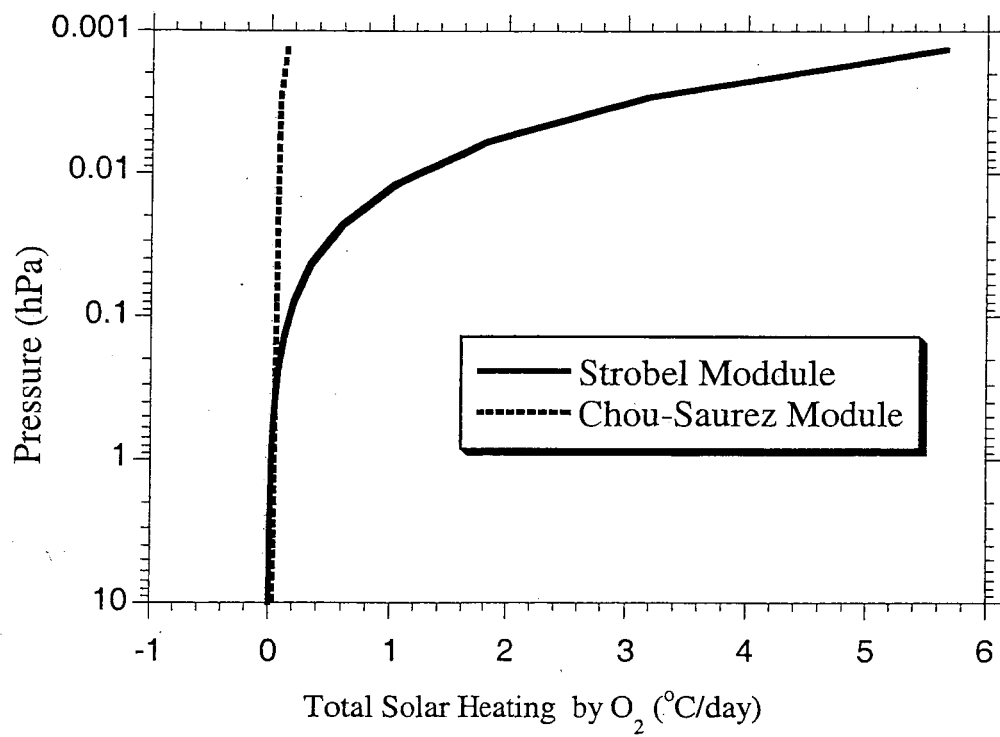


Fig.3

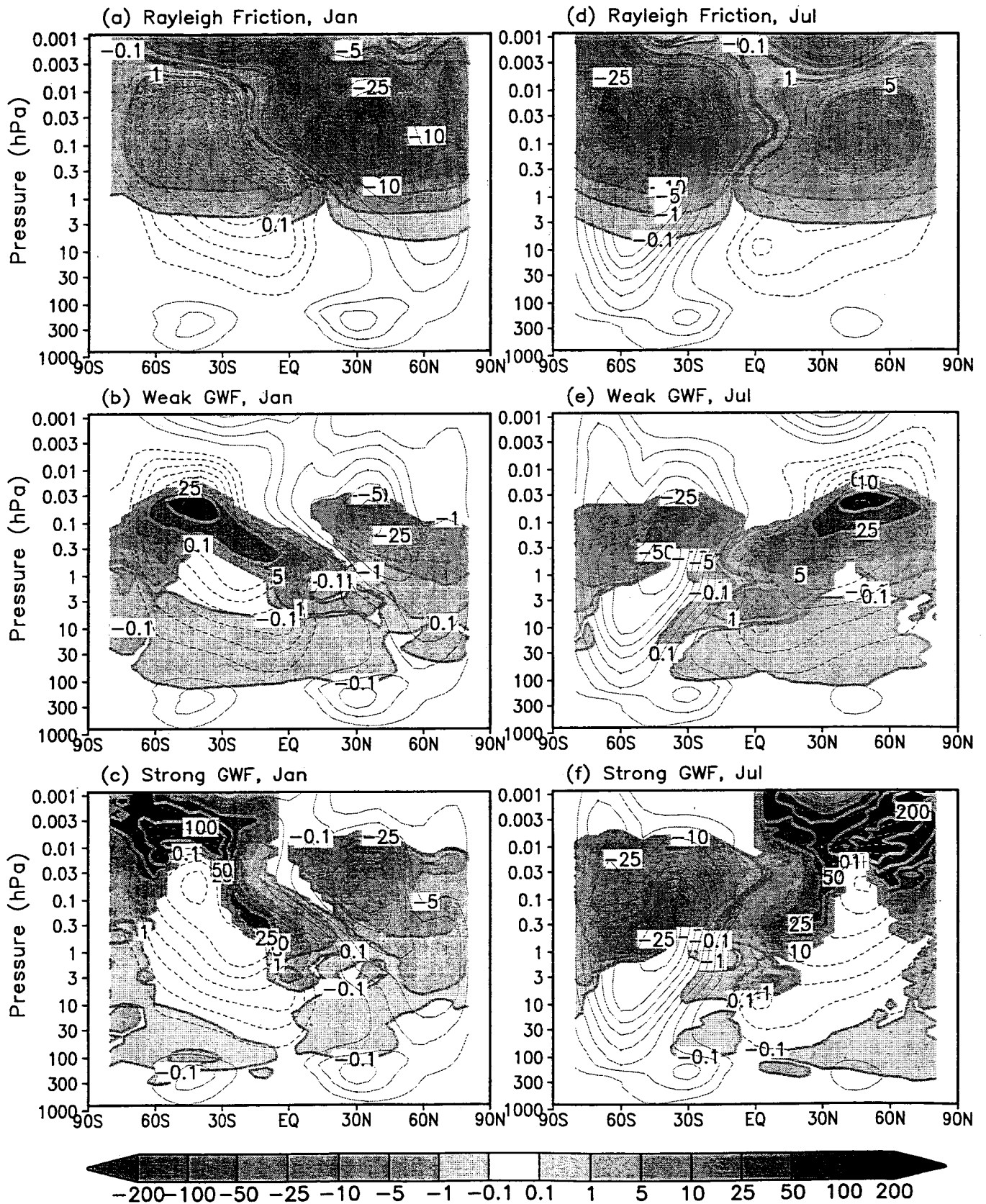


Fig. 4

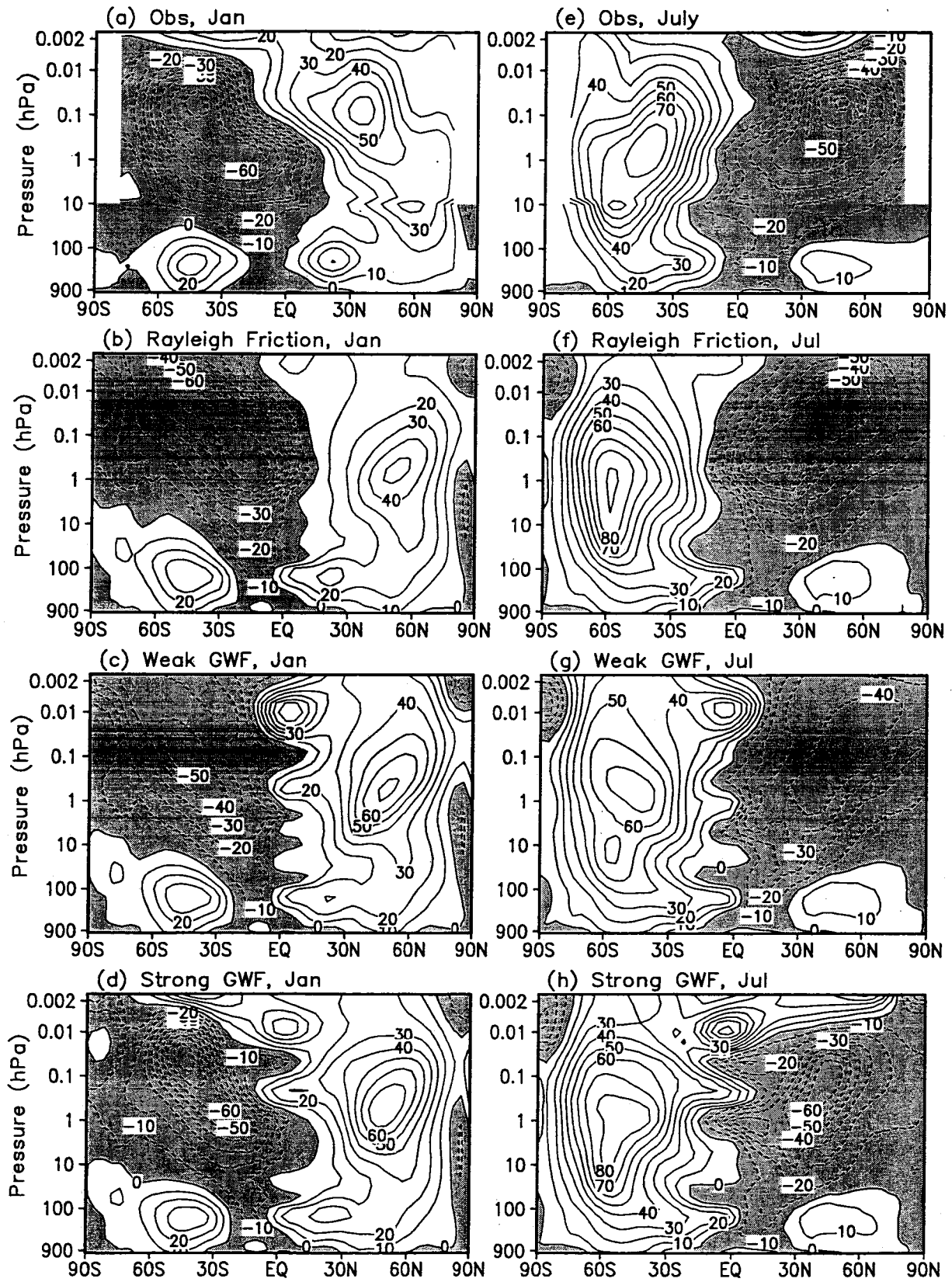


Fig.5

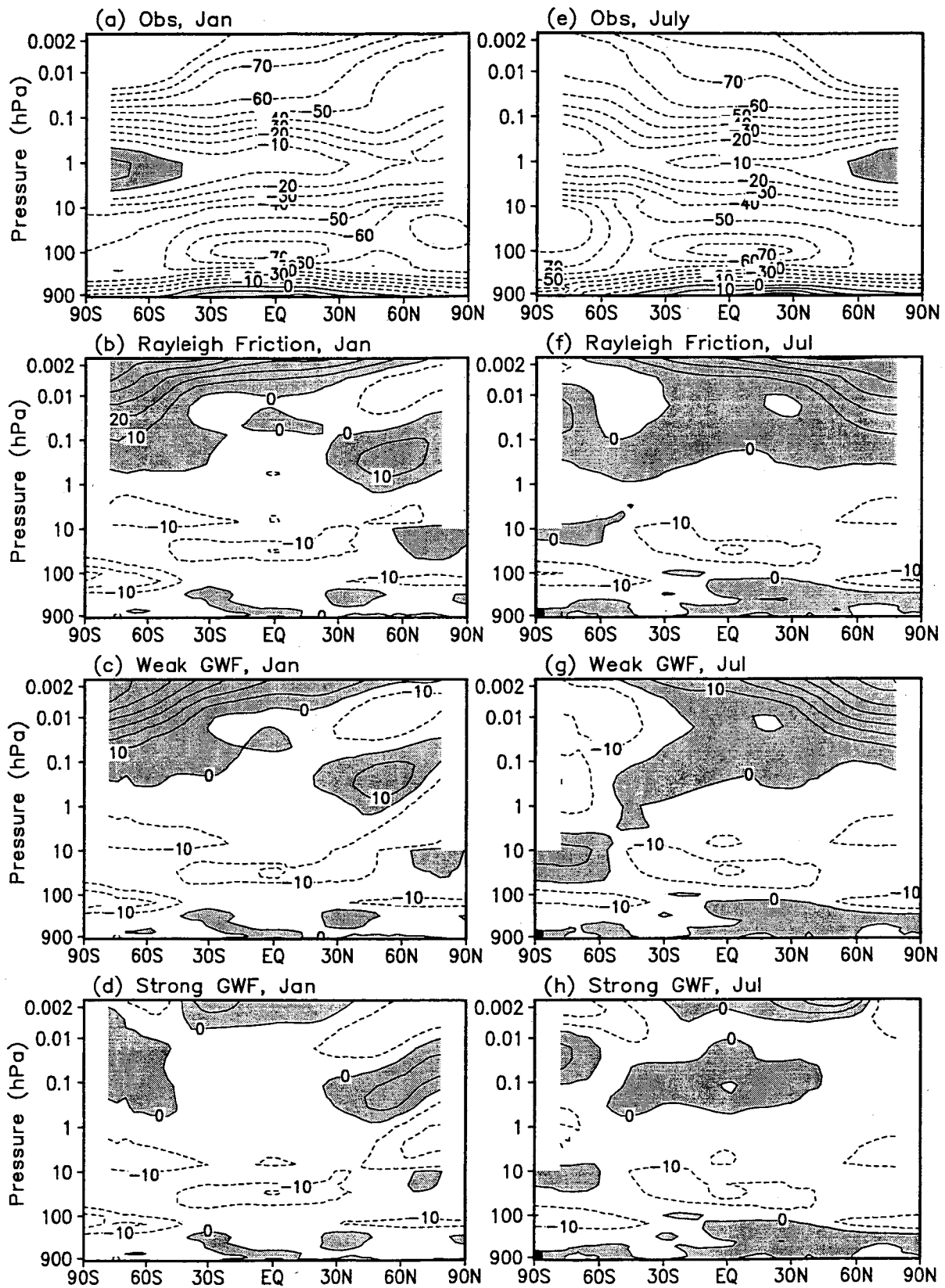


Fig. 6

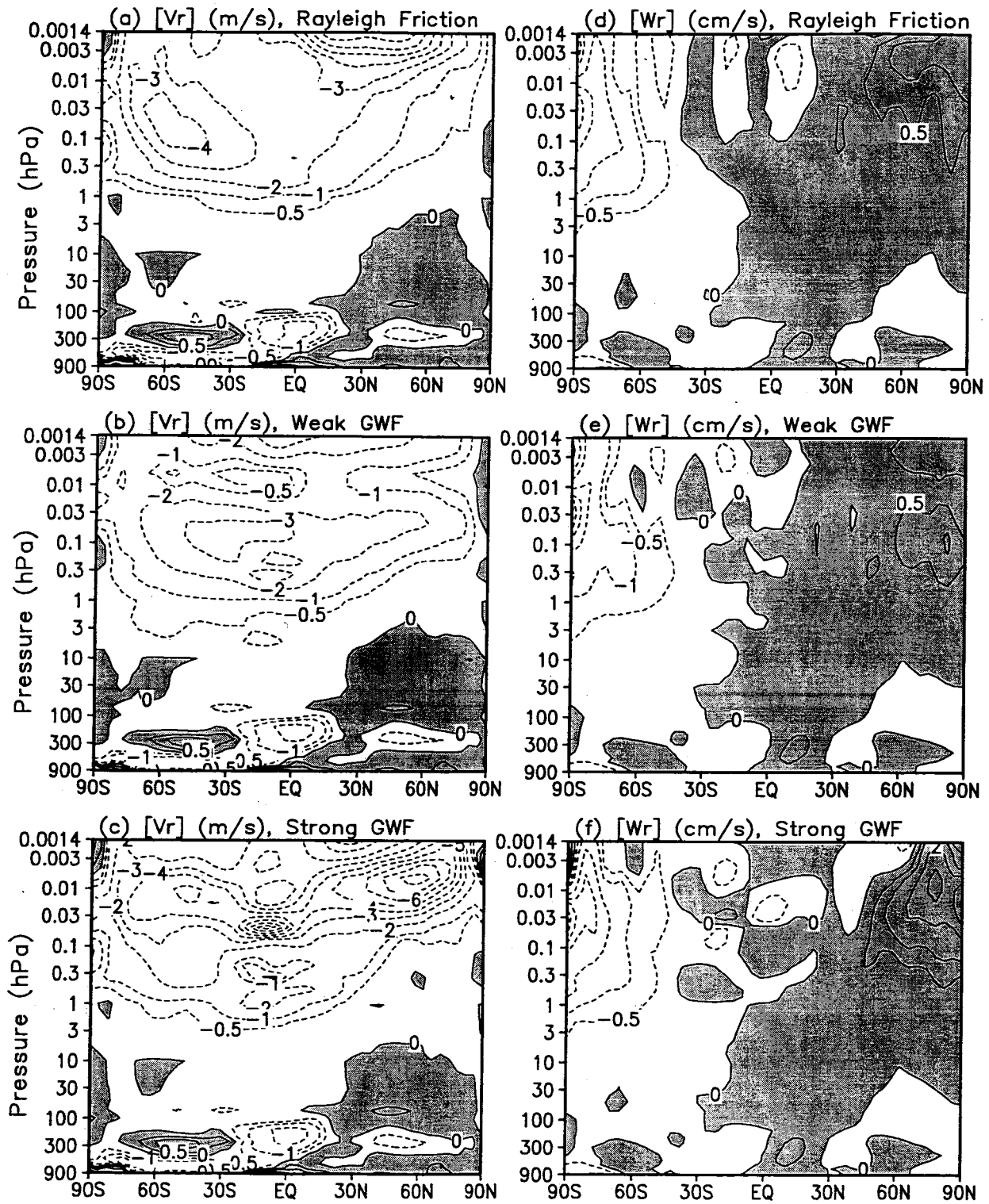


Fig. 7

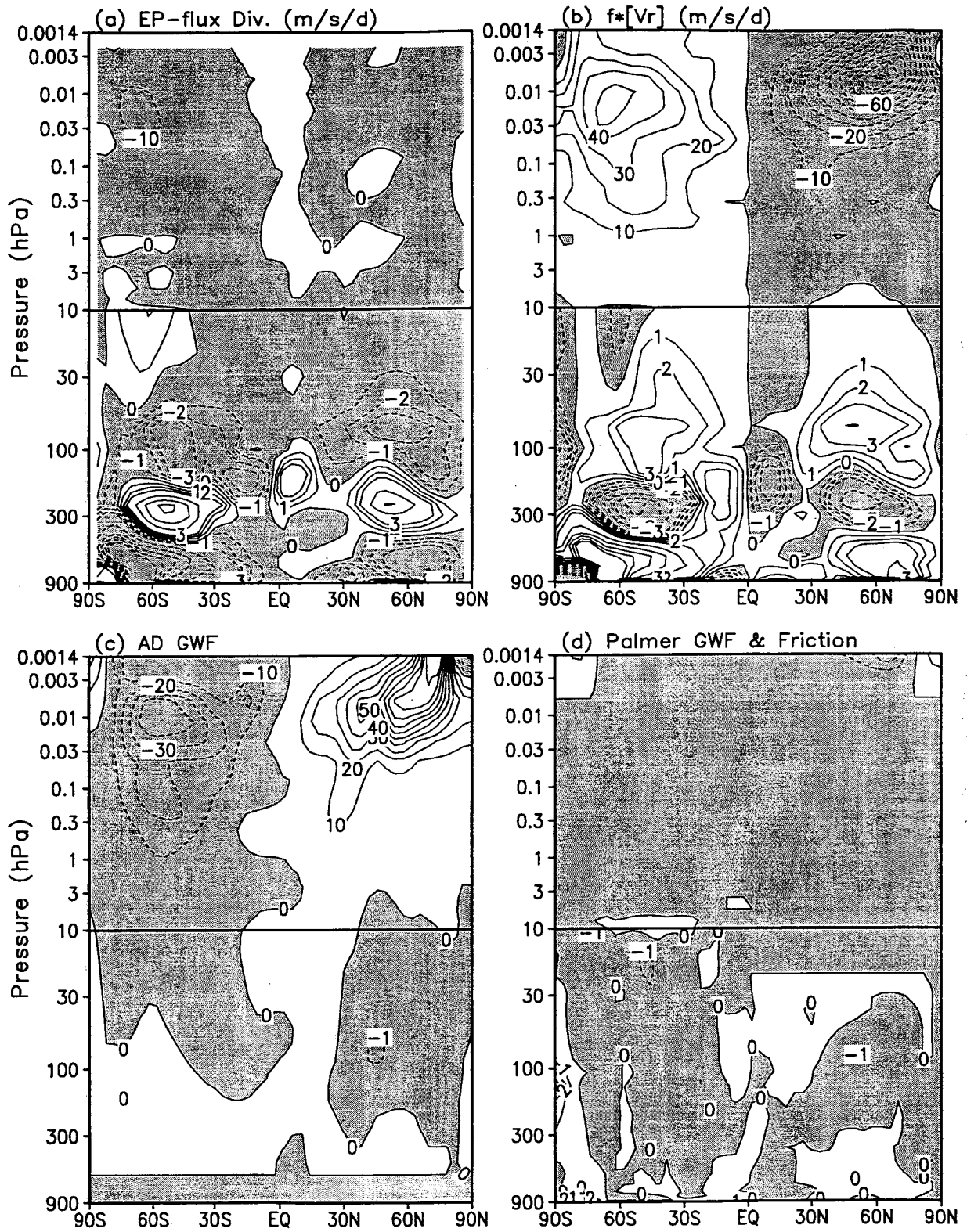


Fig. 8

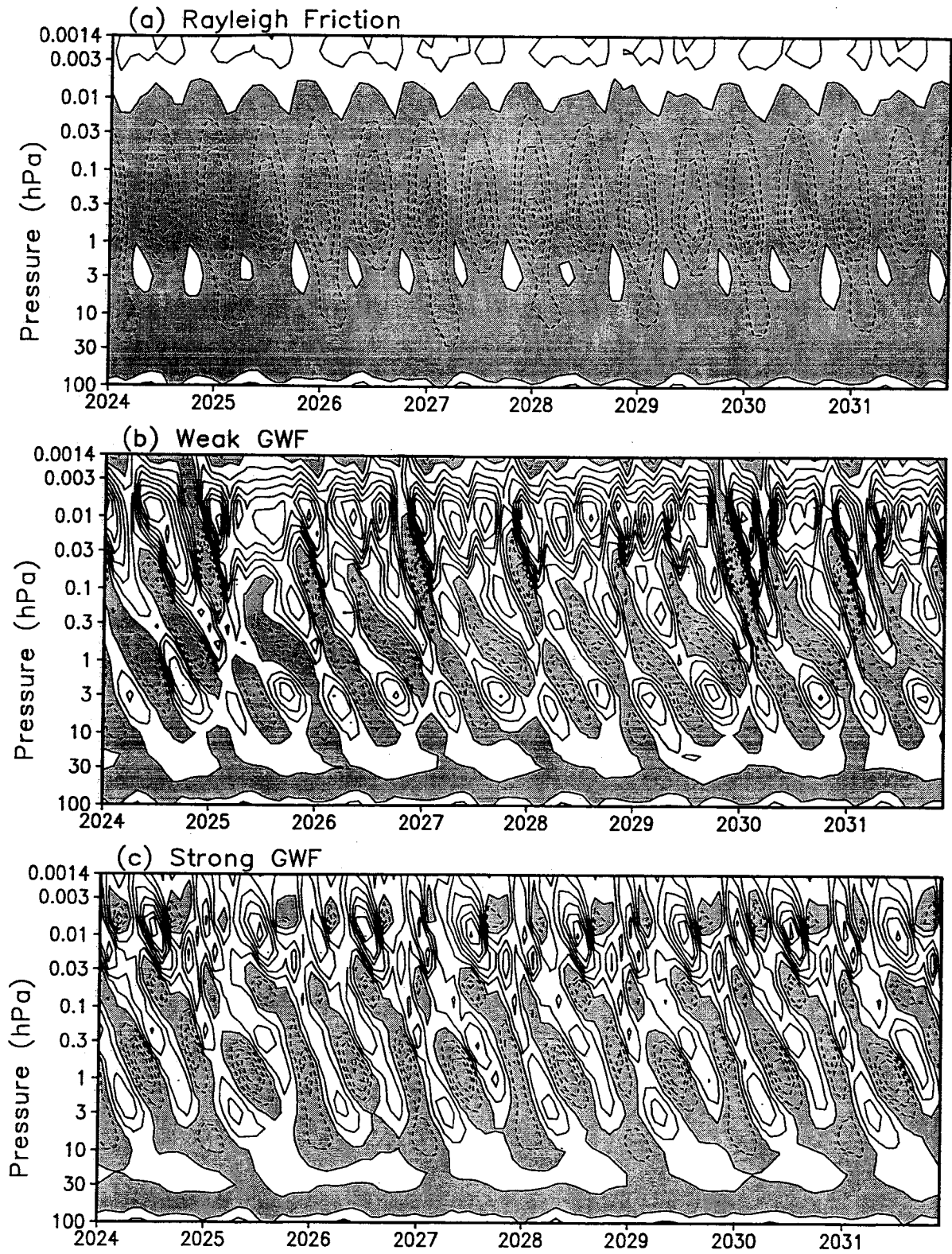


Fig. 9